Polymer 50 (2009) 3302–3310

Contents lists available at ScienceDirect

Polymer

journal homepage: www.elsevier.com/locate/polymer

Heat melding of voided polyethylene microstructures

D.I. Medina [a], F. Chinesta [b], M.R. Mackley [a,*]

[a] Department of Chemical Engineering, University of Cambridge, Pembroke Street, Cambridge CB2 3RA, UK
[b] EADS Corporate Foundation International Chair, GEM, UMR CNRS, Ecole Centrale de Nantes, 1 Rue de la Noe, BP 92101, 44321 Nantes Cedex 3, France

ARTICLE INFO

Article history:
Received 10 November 2008
Received in revised form
6 April 2009
Accepted 19 April 2009
Available online 3 May 2009

Keywords:
Microcapillary films, MCFs
Microcapillary monoliths, MCMs
Heat melding

ABSTRACT

This paper is concerned with the fabrication of voided polyethylene microstructures by heat melding of plastic microcapillary films (MCFs) to form microcapillary monoliths (MCMs), which are consolidated layers of MCFs forming in two-dimensional arrays of microcapillaries. MCMs were manufactured by heat melding multiple layers of low-voidage MCFs or high-voidage MCFs. The optimal conditions for interface adhesion of the MCFs to create MCMs without compromising capillary integrity were investigated.
The MCFs were processed from linear low-density polyethylene (LLDPE) and the melt rheology of the polymer was studied to provide rheological parameters that could be used both to gain an understanding of the character of the polymer and for modeling of the MCM forming process. In particular, the temperature dependent nature of the rheology was investigated at the transition from viscous-dominated behavior to elastic-dominated behavior. Modeling of the melding process provided some additional information and confirmed issues in relation to the thermal bonding temperatures and mechanisms.

1. Introduction

The voided polyethylene microstructures studied in this paper are referred to as a microcapillary film (MCF), characterized by a parallel array of near uniform capillaries embedded within a thin linear low-density polyethylene film as shown in Fig. 1.

Hallmark et al. [1] developed these novel flexible films which have hybrid properties of standard plastic film [2–4], closed-cell polymer foam [5,6] and hollow fibres [7–9]. The manufacture of MCFs was achieved by entraining air within the polyethylene from injection nozzles during the extrusion process at the point where the molten polymer exits the die. The molten films then exit the die with hollow capillaries within the film. Subsequently the film is drawn down and cooled between cooled rollers to form a solid plastic microcapillary film (MCF). Initial processing [1] produced a so called "low-voidage MCF" where the capillary voidage within the final film (of order 15%) was essentially the same as the voidage of the die. Subsequently different kinds of MCFs have been developed such as small diameter low-voidage MCF, high-voidage MCF and ultra-high-voidage MCF [10]. Hydraulic capillary diameters of the MCFs range from 3.5 μm to 5000 μm. The MCFs can be classified according to their capillary diameter as small diameter low-voidage (with capillary of hydraulic diameter of order 3.5 μm), low-voidage (with capillary of hydraulic diameter of order 200 μm), high-voidage (with capillary of hydraulic diameter of order 800 μm).

1.1. Microcapillary monolith

A microcapillary monolith (MCM) is a polymer monolith of MCFs, containing a two-dimensional array of capillaries. The monolith consists of two or more layers of MCFs permanently bonded together over their full length. This multi-layer structure is created by "hot pressing" at temperatures close the melting point of the polymer. This is a delicate process because the temperature, time and load need to be precisely controlled in order to meld the interfaces and to prevent collapse of the hollow capillaries.

The process of MCM formation relies on 'polymer welding', in which two molten or near molten interfaces are bonded together. LLDPE MCFs were heated during the heat welding process in order to create intimate contact between the interfaces enabling polymer chain diffusion to occur across the interface allowing subsequent entanglements to achieve the bonding [11]. The welding process starts when the MCFs are at a temperature close to the melting point of the LLDPE. At this temperature a reduction in the viscosity and entropy occurs, making the mobilization of polymer chains possible, and pressure is applied to facilitate the intimate contact of the MCFs.

The degree of welding and integrity of capillaries in the MCM formation are mainly the function of three factors, the processing temperature, T, applied compression ratio and melding time. The

* Corresponding author. Tel.: +44 0 1223 334784; fax: +44 0 1223 334796.
E-mail address: mrm5@cam.ac.uk (M.R. Mackley).

0032-3861/$ – see front matter © 2009 Elsevier Ltd. All rights reserved.
doi:10.1016/j.polymer.2009.04.051

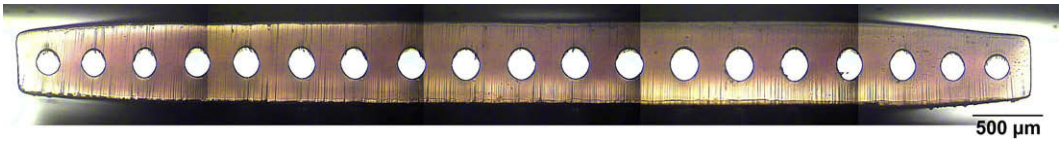

Fig. 1. Optical section of linear low-density polyethylene microcapillary film showing 19 hollow capillaries with capillary mean hydraulic diameters approximately 200 μm.

welding, or healing, which consists of the diffusion of polymer chains across the interface, is dependent on temperature. The MCM melding process was carried out under essentially isothermal conditions and was modeled using the theory of reptation developed by de Gennes [12].

2. Experimental

The linear low-density polyethylene (LLDPE) used was a commercially available grade (Dowlex NG5056E, melt index 1.1 g/10 min, density 0.919 g/cm^3).

Low-voidage MCFs were fabricated according to the method established by Hallmark et al. [1]. The heated extrusion line, shown schematically in Fig. 2, used in the production of 19 capillary films consisted of a single-screw extruder connected to a gear pump. Pressure feedback control was present between the inlet of the gear pump and the motor drive to the extruder's screw. The polymer exited the extrusion line through a heated die with a convergent mid-section that contained air entrainment needles.

Upon exiting the extrusion die, the extrudate was taken through the chill rollers whose position relative to the die exit could be easily altered and act as a variable-speed haul-off device. The distance between the die exit and the chill rollers was termed as the melt drawing length, L_D.

The air entrainment assembly was designed such that the tips of each nozzle were flush with the exit of the die. The die body and 19-injector assembly was attached to the extruder and the extrusion line. The extrusion line was operated at a constant polymer volumetric flow-rate, with the extrudate passing into the rollers and out to the haul-off device. For low-voidage MCFs the final voidage in the MCF film was close to that of the die injector voidage of 15%.

High-voidage MCF was fabricated using a similar process to the low-voidage MCF, but with the difference of using two opposing high speed air jets, which were placed at the die exit to quench the film [10]. The cooling of the molten surface resulted in the internal voidage of the MCF increasing from the die voidage of 10% up to voidage of order 24–70%.

2.1. Low-voidage MCM formation process

The formation of the low-voidage MCM consisted of cutting 30 cm lengths of microcapillary film, placing them on the top of each other and then heat welding them together to form a MCM. The thickness of the MCM would be a function of the number of bonded microcapillary films. The MCFs were placed in an adjustable custom-designed brass mould. The mould consisted of a brass top and an aluminium bottom plate, each 310 mm × 100 mm. The MCM thickness was controlled with brass spacer strips, which were 0.051 mm, 0.52 mm, 1 mm and 5 mm thick. A heated press (Moore E1322) was used in order to obtain a controlled claming load (Fig. 3a). The following procedure was used: The multi-layer stack of MCFs was prepared by layering the specific amount of MCFs on top of each other, the MCFs were held together using tape.

The thickness of the untreated stack (t_o) and thickness of the mould (t_m) were measured. The brass mould was adjusted to t_m using the brass strips. A compression ratio was calculated from t_o and t_m (see Equation (1)).

$$C_R = \frac{t_o - t_m}{t_m} \tag{1}$$

The untreated stack was loaded into the mould at room temperature. After that the mould was introduced into the hot press with no applied load, but in contact with the two plates, for 6 min to allow temperature equilibration (Fig. 3b). Finally, after a melding time of 5 min at a constant temperature, and a load of 4 tonnes (Fig. 3c) the pressure was released and the plates were taken out of the press and allowed to cool down before opening the mould.

2.2. High-voidage MCM formation process

The manufacture of high-voidage MCMs was similar to the low-voidage MCM, with the differences of temperature, load and welding time parameters together with the use of a polymer film interlayer. Optimal parameters in order to avoid collapse or deformation of the capillaries were established.

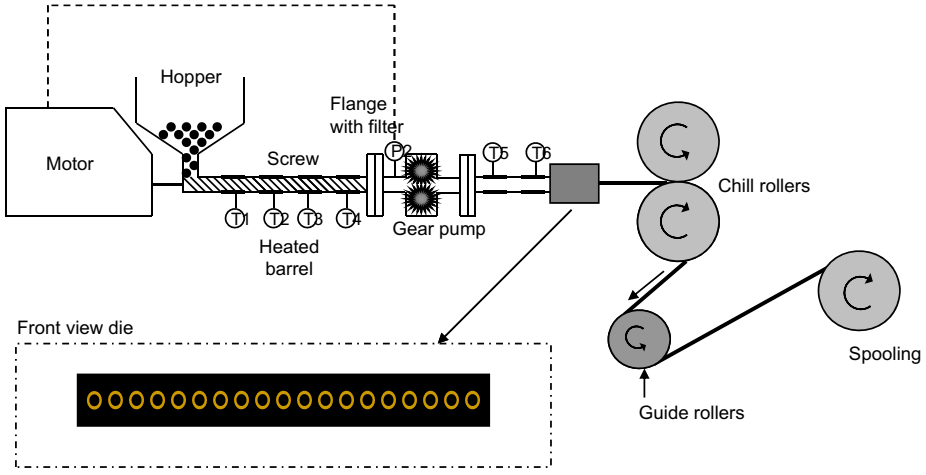

Fig. 2. Extrusion processing of microcapillary films.

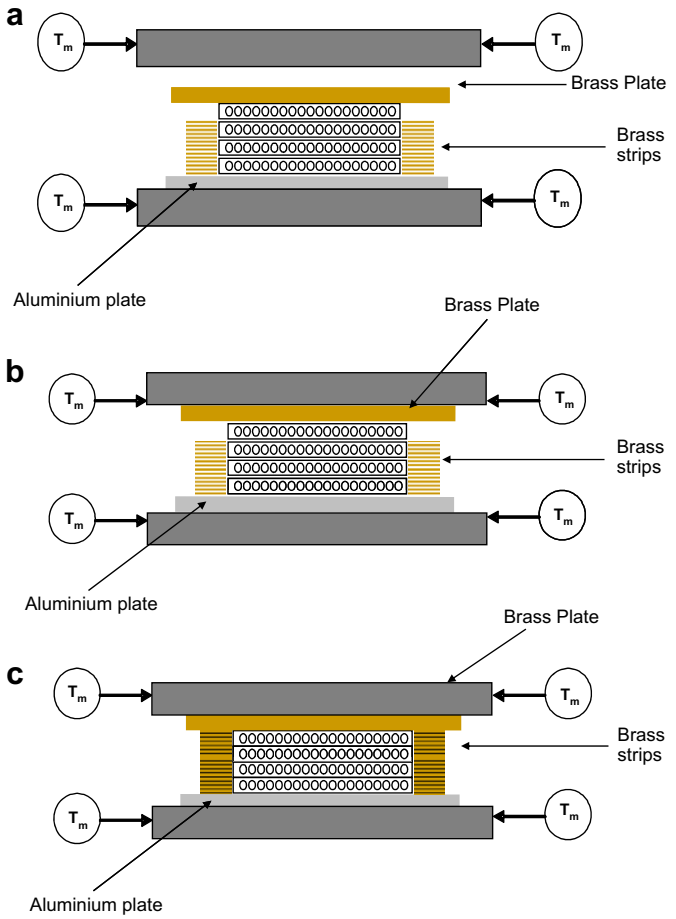

Fig. 3. Schematic diagram of (a) MCM moulding consisting of heat plates, a brass top and an aluminium bottom plate, (b) MCM mould in the heat press with no applied load but in contact with the two plates for 6 min, and (c) MCM mould in the heat press with a load of 4 tonnes for melding time of 5 min.

2.3. Rheological characterization

Rheological characterization experiments were carried out to obtain material parameters that describe the linear, non-linear viscoelastic response and temperature dependence of the base polymer.

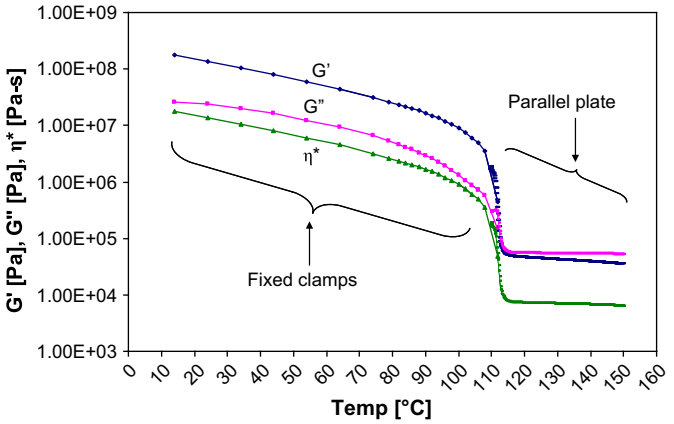

Fig. 5. The temperature dependent nature of the LLDPE NG5056E rheology. Identifying the transition from viscous-dominated behavior to elastic-dominated behavior.

The melt processing properties were investigated by performing shear rheometry. An Advanced Rheometric Expansion System rheometer (ARES-LC model 5450DT), was used to carry out these experiments. A stepper motor drives the lower plate in oscillation, while the upper plate is connected to a transducer, which measures torque and normal force (Fig. 4a). In dynamic experiments, shear strain, resultant shear stress and the phase angle between these are resolved. As a result the elastic and viscous moduli can be calculated.

The ARES rheometer was configured with 25 mm diameter parallel plates and heated by an air-blast oven. For the solid samples a rectangular/torsion fixture was used as shown in Fig. 4b. Rectangular samples (of dimensions $x = 1.5$ mm, $y = 12$ mm, $z = 30$ mm) were mechanical gripped and tested in a similar way to the melt.

Differential Scanning Calorimetry (DSC) was carried out on a Pyris 1 Perkin Elmer 300VA calorimeter with heating and cooling rates of 10 °C/min over the temperature range 0–200 °C. The ramp rate of 10 °C/min was chosen to minimise structural reorganisation during heating whilst ensuring that reliable melting temperatures could be obtained [13].

The sensitivity of the DSC was 0.0001 mg. Samples with mass in the range 7.00 ± 0.50 mg were cut from the low-voidage MCF and HV-MCF samples.

In order to establish the capillary size, shape and interfacial bonding of the MCFs a visual characterization technique was used.

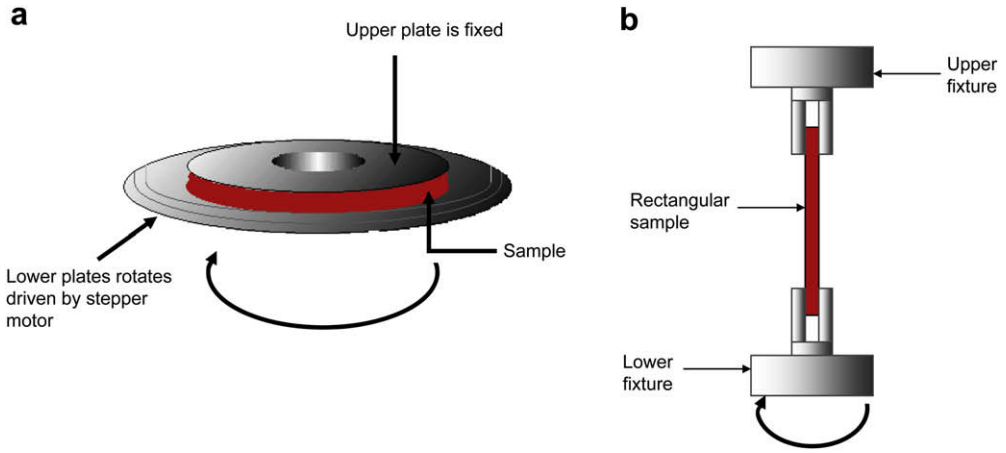

Fig. 4. ARES rheometer used to carry out rheology characterisation experiments (a) parallel plate geometry for high temperature experiments and (b) rectangular/torsion fixture for low-temperature experiments.

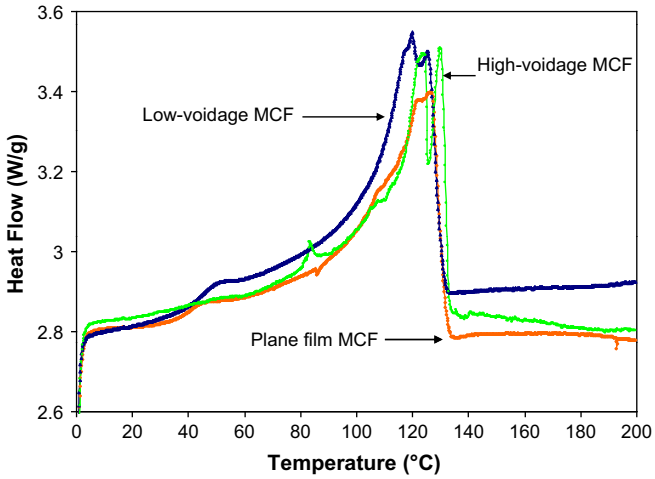

Fig. 6. Differential scanning calorimetry showing the melting endotherm for LLDPE NG5056G. (a) Low-voidage MCF, (b) high-voidage MCF and (c) plane film.

An optical microscope Olympus BH-2 allowed effective detailed mapping of the MCFs capillaries size, shape and distribution along the film. A graticule was photographed and used to determine the film thickness and capillary size. These results were confirmed by JEOL 6340F Scanning electron microscopy (SEM) with an accelerating voltage of 5 kV.

3. Results and discussion

The rheology and DSC data are shown in Figs. 5 and 6 respectively. These data show that for this polymer a melting transition occurs at around 114 °C and it is in this temperature region that melding experiments were carried out.

3.1. Low-voidage MCF melding

Fig. 7 is an example of extreme melding conditions. If melding is carried out at 124 °C as shown in Fig. 7a there is complete collapse of the capillaries. By contrast if melding is carried out at 100 °C as shown in Fig. 7b, no interface bonding occurs. Clearly intermediate conditions are required and these are mapped out in Fig. 8. The figure shows optical sections of MCM obtained for different compression ratios and melding temperatures. All were taken for a 300 s melding time. The figure shows optimum interface formation whilst retaining capillary integrity of order $T = 114–120$ °C and $C_R = 0.26–6.82\%$. The diagonal cross-hatched zone indicates too weak interfacial bond and the horizontal hatched zone, partial capillary distortion. The optimum interface formation condition is close to the peak in the DSC trace and also at the cross over to the G', G'' trace.

3.2. High-voidage MCFs

By virtue of its greater voidage, the high-voidage MCF is more susceptible to loads than the low-voidage MCF and in addition fundamental differences in interface bonding were discovered. Fig. 9 shows a series of high-voidage MCM sections for melding at similar conditions to the low-voidage examples. Two things are noticeable; the collapse of the capillaries as shown in Fig. 10 and the poor interface bonding. Increasing the temperature or bonding time did not enable bonding to occur without capillary collapse.

It was suspected that the high-voidage interface behaved in a different way to the low-voidage interface and X-ray measurements shown in Fig. 11 indicated that the high-voidage MCFs were oriented and the low-voidage were not. The DSC curve in Fig. 6 also shows that the high-voidage MCF has a higher melting point. It appears that orientation reduces the melding ability at these intermediate temperatures and it was not found possible to form high-voidage MCMs in the same way as low-voidage MCMs were achieved.

An effective way of forming high-voidage MCMs was discovered; a plane film of LLDPE was used as an interlayer between adjacent MCFs. This is shown in Fig. 12 where conditions were found for good interface bonding and also capillary integrity.

3.3. Modeling of MCM formation

A number of aspects for the low-voidage MCM bonding have been modeled including the development of the MCM, thermal profile, capillary distortion due to an uneven interface and reptative polymer diffusion across an interface. The modeling is far from complete but it does help to understanding some of the physical issues involved.

3.4. Thermal modeling

The heating temperature kinetics of the MCF stack was calculated and compared with the measure kinetic. A schematic of the geometry is shown in Fig. 13 and the heat differential Equation (2) given below was numerically solved.

$$\frac{\partial^2 T}{\partial x^2} + \frac{\partial^2 T}{\partial y^2} = \frac{\rho Cp}{\lambda}\frac{\partial T}{\partial t} \tag{2}$$

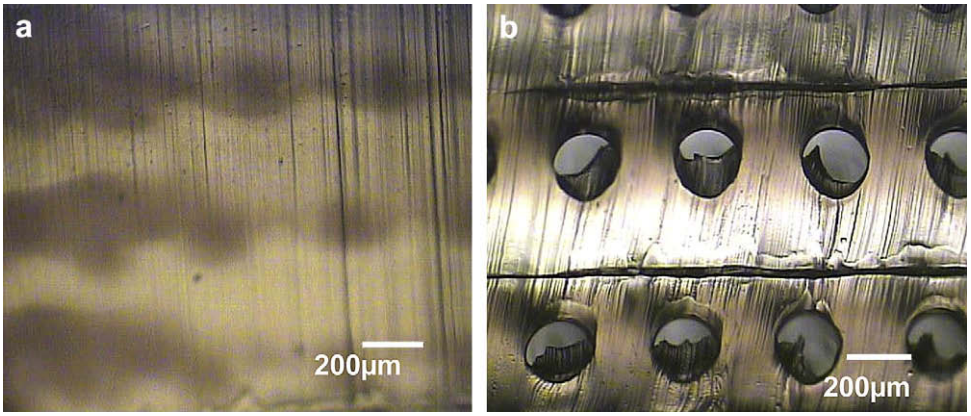

Fig. 7. Cross-sectional view of low-voidage MCMs carried out at extreme conditions of welding temperature and compression ratio, (a) $T = 124$ °C with CR = 6.82 % and (b) $T = 106$ °C with CR = 0.26 %.

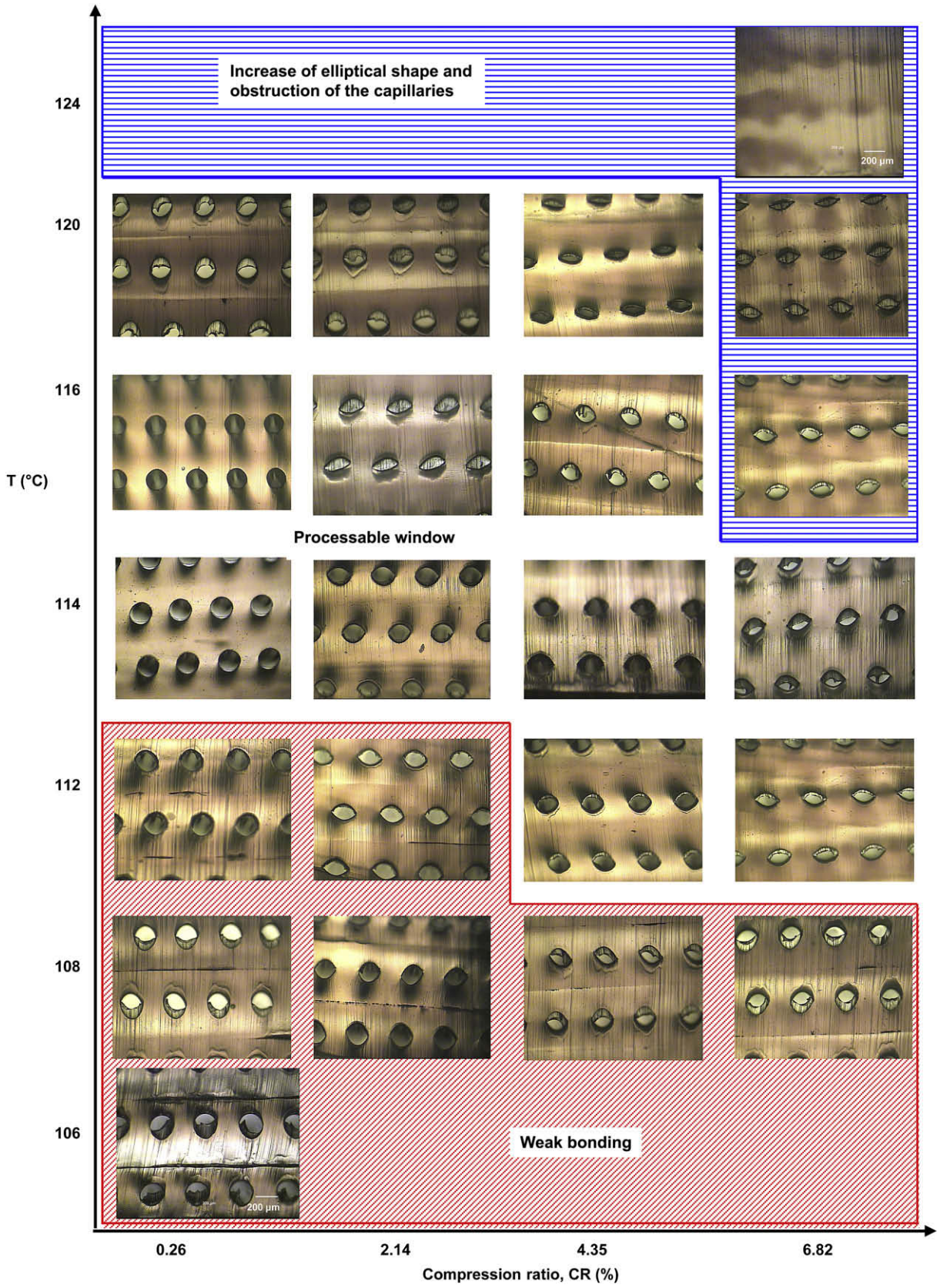

Fig. 8. Results of low-voidage MCM bonding as a function of temperature and compression ratio for a compression time of 300 s. Weak bonding zone shown as diagonal cross hatch. Capillary collapse shown as horizontal hatching. Optimum MCM formation conditions: $T = 114–120\ ^{\circ}C$, CR = 0.26 %, time = 300 s.

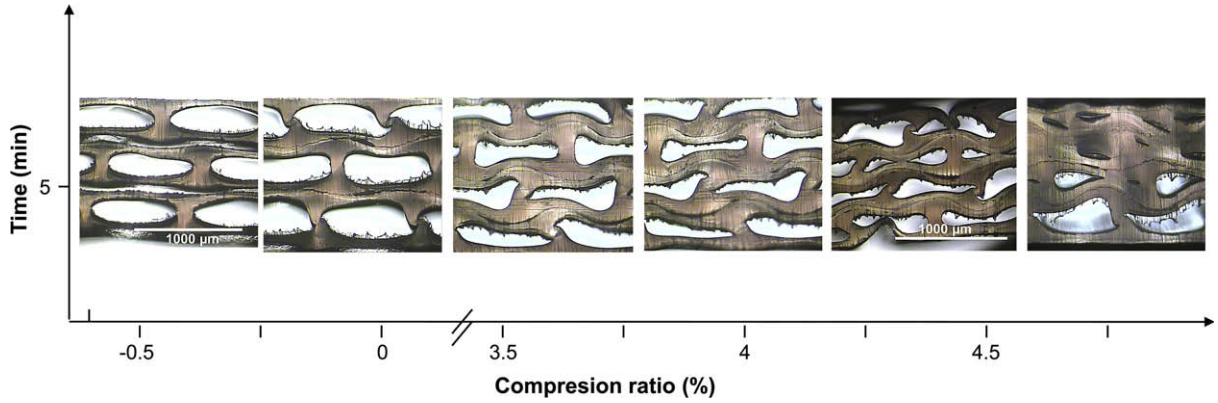

Fig. 9. Photographs showing high-voidage MCM bonding as a function of compression ratio at a temperature of 114 °C after a moulding time of 5 min.

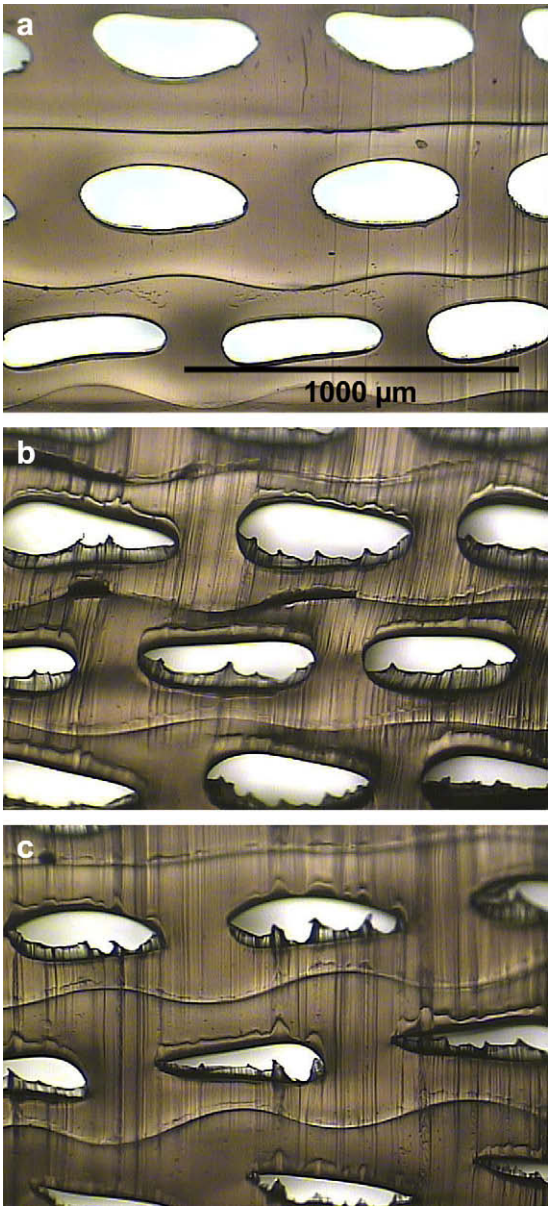

Fig. 10. High-voidage MCM bonding at (a) 114 °C, compression ratio of approximately 3% for a bonding time of 30 min, (b) 116 °C at compression ratio of 2% for a bonding time of 10 min and (c) 116 °C at 3% for a bonding time of 10 min.

where T is the temperature of the MCM at coordinates x and y at specific time t, ρ is the density, Cp is the specific heat capacity and λ is the thermal conductivity for the MCF.

The experimentally measured input surface oven plate was introduced as a boundary condition and the temperature rise kinetic of both mould plates and MCF stack established. The numerical results agree well with the experimental thermocouple temperature profile positioned at the centre of the stack as shown in Fig. 14. The modeling showed that most of the thermal resistance came from the heating of the mould and not the MCF itself.

3.5. MCF interface modeling

The surfaces of the MCFs were not perfectly flat and an essential part of the good interface bonding between adjacent MCF surfaces was to have a good contact. A minimum value of compression ratio was necessary to achieve good contact, however if the compression ratio was too high distortion of the hollow capillaries occurred.

In an attempt to gain some insight into this process mechanical numerical modeling was carried out on an elastic MCF with smooth boundary conditions on one side and an irregular boundary on the other. The geometric section of MCF and boundary is shown in Fig. 15.

The thermomechanical model was solved numerically assuming the Young modulus $E = 2.5E5$ Pa and Poisson ratio $\nu = 0.45$. Fig. 16 shows the distortion of the capillaries for a compression ratio deformation of 5.9%. The results show that if one of the surfaces is irregular, distortion of the capillary holes will occur. In general this was not seen experimentally except in the case of the high-voidage MCM where capillary collapse occurred. In reality some plastic distortion almost certainly occurs at an uneven interface when a load is applied and this will need to be included in future modeling.

3.6. Interface bonding

The modeling of the interfacial bonding is difficult unless the two surfaces are considered as molten polymers of unique molecular weight and that the surfaces are in perfect physical contact. The reality is that the surfaces are not necessarily in perfect contact and the polymer contains a distribution of molecular weights. The polymer chains are not in the fully molten state and that partial crystallinity influences the bonding process. The fact that the oriented high-voidage MCF had different bonding characteristics to the unoriented low-voidage MCF also demonstrates that interfacial bonding in the temperature regime considered has considerable complexity.

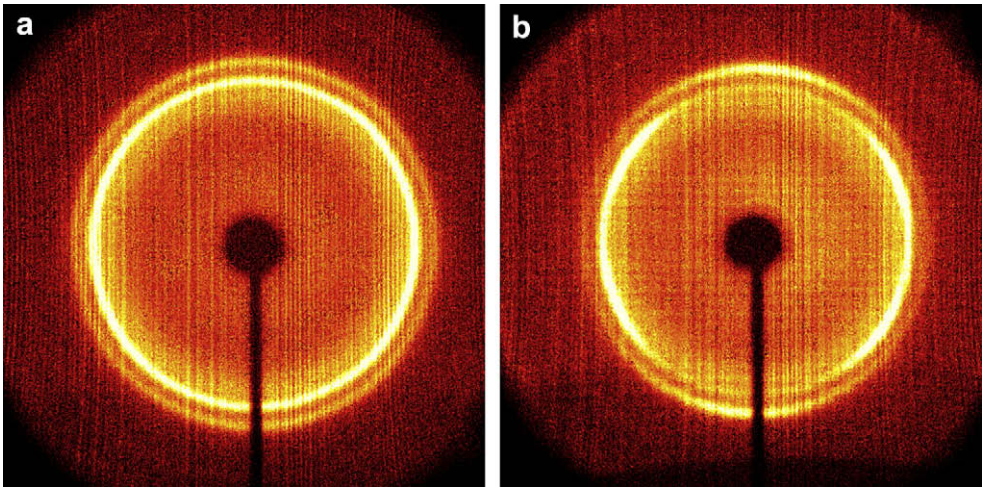

Fig. 11. LLDPE WAXD pattern of (a) low-voidage MCF and (b) high-voidage MCF. Extrusion axis vertical.

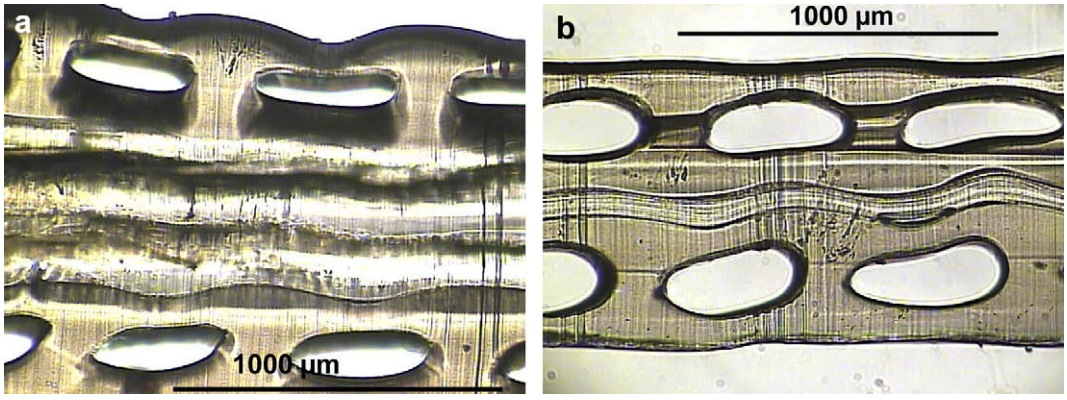

Fig. 12. High-voidage MCM fabricated at a bonding temperature of 114 °C, compression ratio of 1% for a compression time of 5 min, using (a) plane film of thickness 0.6 mm between high-voidage MCFs and (b) thinner polyethylene plane film of initial thickness of 0.07 mm.

If a pure melt and perfect interface assumption is assumed, progress can be made in relation to modeling. The reptation concept of de Gennes [12], provides a framework for analysis [14]. The reptation diffusion Equation (3) can be solved

$$\frac{\partial P}{\partial t} = D\frac{\partial^2 P}{\partial s^2} \tag{3}$$

where P is the probability density function, which is related to the position s of a chain segment at time t, D is the temperature dependant reptation diffusion constant, the diffusion constant depends on the length of the chain L by an Equation (4) [15]

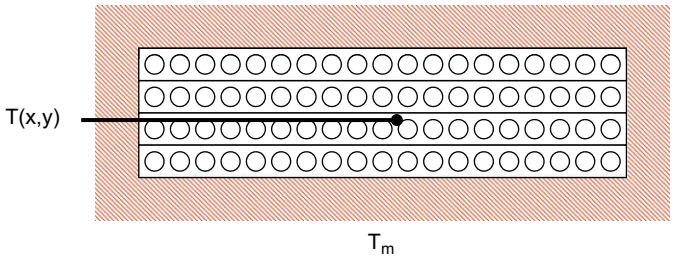

Fig. 13. Heat conduction schematic of the low-voidage MCM.

$$t_R(T_o) = \frac{L^2}{2D_o} \tag{4}$$

where t_R is the reptation time, L is the total length of the chain and D_o is the isothermal reptation coefficient at temperature T_o.

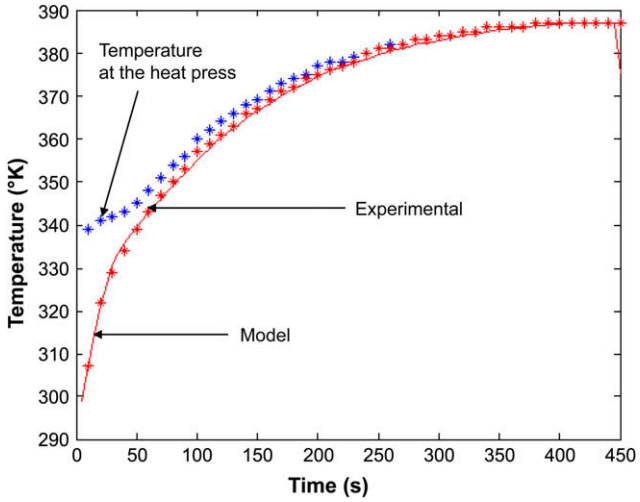

Fig. 14. Plot of temperature change as a function of time for an MCM formed with four MCFs. Experimental heat press and surface temperature shown together with model predictions.

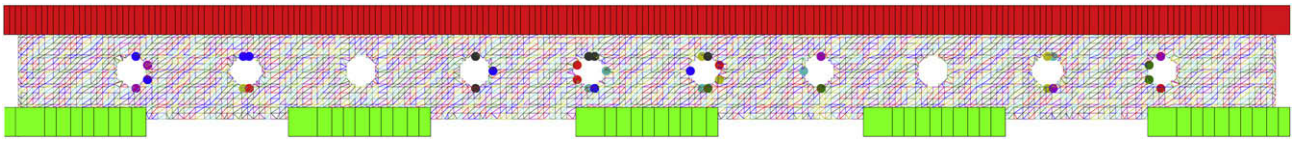

Fig. 15. Model representation of a low-voidage MCF showing simulation grid network. Smooth upper boundary represents metal plate and structured lower boundary approximates surface roughness of lower MCF laminate.

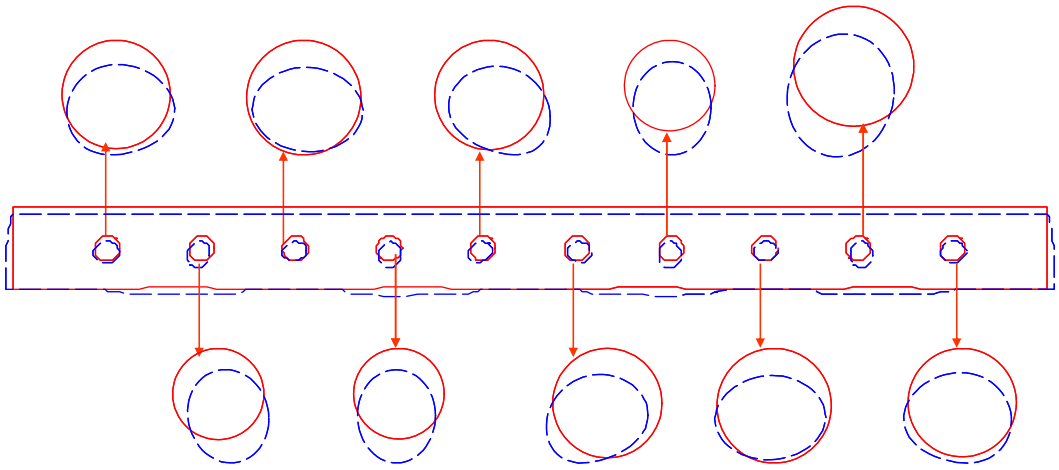

Fig. 16. Simulation of a low-voidage MCM capillaries subject compression ratio of 5.9%. — undeformed state and - - - deformed state.

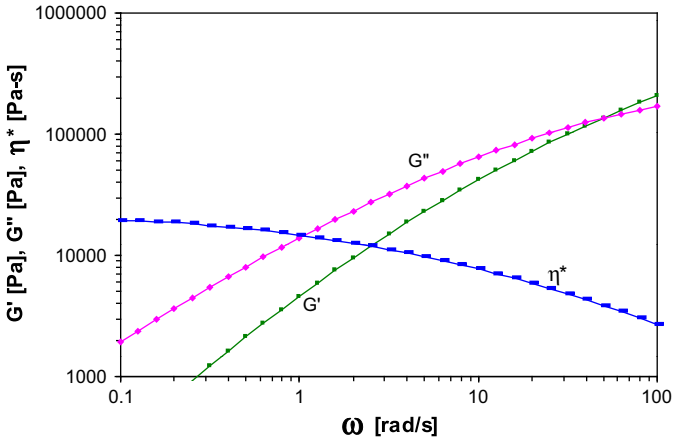

Fig. 17. Dynamic frequency sweep for LLDPE NG5056E at 140 °C and strain of 1%.

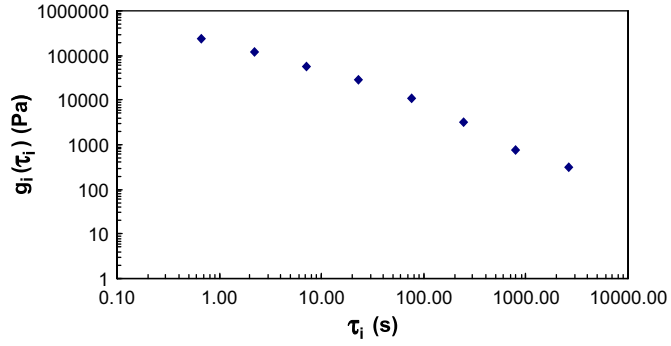

Fig. 18. Relaxation spectrum of LLDPE NG5056E at 140 °C

Equation (5) shows the relationship between the minor chain length, the total chain length and the time of reptation [12,15,16].

$$\frac{l^2}{L^2} = \frac{t}{t_R} \tag{5}$$

Modeling the melding process at temperatures close to the melting point of the polymer is extremely difficult. The model requires knowledge of the reptation time for the polymer at the applied melding temperature. It is possible to obtain relaxation spectrum for the polymer used in this study at temperatures above the melting point. Fig. 17 shows the frequency sweep at 140 °C, and using a software program RepTate [17], the longest relaxation modes can be identified as shown in Fig. 18. This has been carried out for each temperature above the melting point and a plot is shown in Fig. 19.

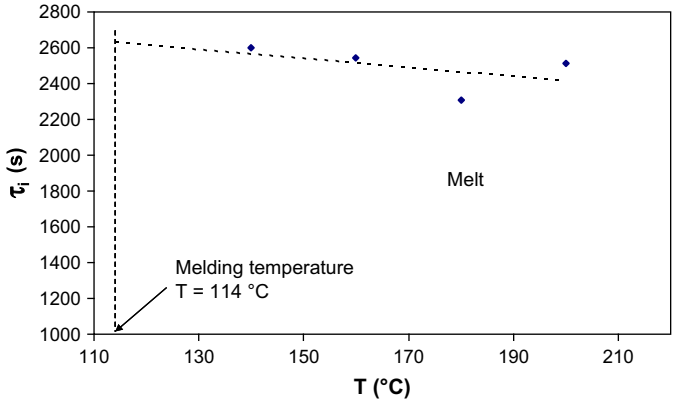

Fig. 19. Longest relaxation modes identified using a software program reptate from relaxation spectrums for the polymer used in this study at temperatures above the melting point.

If these data are extrapolated to the melding temperature a reptation time of τ_R of 2632 s is obtained. This almost certainly is an underestimate of the true reptation time at that temperature because the material is still partially crystalline.

The advancement of the diffusion of the chains to the interface, N, can be calculated with the following equation:

$$N = \frac{t}{t_R} \tag{6}$$

Complete reptation at 114 °C therefore is predicted to occur at 2632 s, however experimentally it was found that melding of the MCF interfaces occurred within 300 s. This result suggests that complete reptation is not necessary in order to establish what appears to be a uniform interface. The simple reptation concept is not adequate in order to explain the differences found for low and high-voidage MCM formation where the orientation of the high-voidage MCF meant that an unoriented polymer interlayer film had to be used.

4. Conclusions

This paper has established melding conditions where plastic microcapillary film (MCF) can be bonded together to form a 2D microcapillary monolith (MCM). The problem is a delicate one as if too low temperature is applied the MCFs will not bound, however if too high a temperature is used the polymer melts and the hollow capillaries collapse. A reasonably wide processing window for low-voidage MCF was established in relation to moulding temperature, compression ratio and time.

High-voidage MCFs have intrinsic molecular orientation associated with the quench forming process and because of this orientation it was found difficult to establish a processing window where good interbonding could be achieved. The problem was partially overcome by using an unoriented plane film interlayer.

Rheological data for the LLDPE used to form the MCM have been presented over a temperature range that covers the materials solid and melt behavior. In particular the region near the melting point brings particular difficulties in measurement, however it is in this region where the melding process occurs.

The formation of MCM was partially modeled by solving the transient heat transfer problem, analyzing the deformation of MCF under load and also examining interfacial reptation diffusion. Overall a picture emerges where a viable processing window can be identified in order that MCMs can be fabricated.

MCMs may have future applications for MCFs when used for heat transfer, microreactors or other usage. The transition temperature behavior of polyethylene presented in the paper has general relevance to polyethylene forming process at and around the melting range of the polymer.

MCFs are being developed as microreactors where MCFs were heat melded to form microflow discs (MFD)s [18]. The joining of different streams A and B involves melding MCFs to form MCMs. In addition the manufacture of heat exchangers from MCFs also involves the melding of MCFs to form monolith structures.

Acknowledgements

Dora I. Medina would like to thank CONACyT for financial PhD support and Malcolm R. Mackley would like to thank EPSRC for financial support of MCF development.

References

[1] Hallmark B, Gadala-Maria F, Mackley MR. Journal of Non-Newtonian Fluid Mechanics 2005;128(2–3):83–98.
[2] Briston JH, Katan LL. Plastics films. 1st ed. London: The Plastics Institute; 1974 [part 2].
[3] Han CD. Rheology in polymer processing. 1st ed. New York: Academic Press Inc; 1976. p. 366.
[4] Zatloukal M, Vlcek J. Journal of Non-Newtonian Fluid Mechanics 2006;133(1):63–72.
[5] Mills NJ, Zhu HX. Journal of the Mechanics and Physics of Solids 1999;47(3):669–95.
[6] Zhu HX, Mills NJ, Knott JF. Journal of the Mechanics and Physics of Solids 1997;45(11–12):1875–904.
[7] Dees JR, Spruiell JE. Journal of Applied Polymer Science 1974;18(4):1053–78.
[8] White J, Cakmak M. Advances in Polymer Technology 1986;6(3):295–337.
[9] Syang-Peng R. Journal of Applied Polymer Science 2001;82(12):2896–902.
[10] Medina DI, Hallmark B, Lord TD, Mackley MR. Journal of Materials Science 2008;43(15):5211–21.
[11] Grewell D, Benatar A. International Polymer Processing 2007;22(1):43–60.
[12] de Gennes PG. Journal of Chemical Physics 1971;55(2):572.
[13] Wunderlich B, Czornyj G. Macromolecules 1977;10(5):906–13.
[14] Gao P, Mackley MR. Polymer 1994;35(24):5210–6.
[15] Yang F, Pitchumani R. Macromolecules 2002;35(8):3213–24.
[16] Wool RP, Yuan BL, McGarel OJ. Polymer Engineering and Science 1989; 29(19):1340–67.
[17] Ramirez J, Likhtman A. RepTate – Rheology of Entangled Polymers Toolkit for the Analysis of Theory and Experiments. muPP2 project; 2008.
[18] Hornung CH, Mackley MR, Baxendale IR, Ley SV. Organic Process Research and Development 2007;11(3):399–405.